LONG-TERM CALIBRATION OF WIND AND WAVES IN THE MEDITERRANEAN SEA

L.CavalerI, L.Bertotti, and M.Sclavo

ISDGM-CNR, S.Polo 1364, 30125 Venice, Italy

INTRODUCTION

We have faced the task of assembling a very accurate data set of wind and wave data in the Mediterranean Sea. The Mediterranean is a very active basin, whose meteorology is dominated by the contrasting climates at its southern and northern borders, The hot climate of North Africa contrasts markedly with the stormy weather of Central and Southern Europe. Most of the storms come from the North-West sector, while relatively frequent inflows of Siberian air bring cold north-easterly winds on the northern part of the basin. These storms can reach the African coast, but with a reduced strength. The latter part of the basin is interested by southerly winds (sirocco, kamsin) which can bring warm southerly storms up to the northern part of the Mediterranean Sea. The complicate orography all along most of the borders makes the evaluation of the surface winds a difficult challenge, with a strong variability both in space and time. As it will be shown in the section in the results, this has implications on the accuracy of the available model data.

During the last decade satellite data have become more and more common. They provide a wealth of information, with the further advantage of being weather independent. They measure preferably in the open sea, off the coast. From the point of view of an atlas, one limitation is the time interval with which the data are measured, the choice when defining the orbit being between a more dense coverage sparse in time or more frequent passes at larger space interval.

The only source that provides a complete and dense coverage in space and time is numerical modelling. Both meteorological and wave models have reached a high degree of sophistication. Available from the archive of the various meteo-oceanographic centres, they can confidently be used for long term statistics. However, while the quality of the meteorological output is very high, the surface winds, the ones we care about for oceanographic and navigation purposes, tend to be more affected by the proximity of land. In these areas, and particularly in the enclosed basins like the Mediterranean Sea, the standard model data do not stand by themselves for a reliable statistics.

The solution comes in the combined use of both the model and satellite data. The model data provide the coverage, in time and space, while the satellite provide the required accuracy. Therefore the technique consists in using the satellite data to calibrate the model data, which are then used to evaluate the required statistics.

THE DATA SOURCES

We have made used of the model data from the archive of the European Centre for Medium-Range Weather Forecasts (ECMWF, Reading, U.K.). The Centre produce daily meteorological forecasts and analysis data, the latter ones representing the best possible estimate of the situation at a given time. Since July 1992 ECMWF run also a wave model, whose input information are the surface winds provided by the meteorological model. Both these models are run on a global scale (see Simmons, 1991 and Komen et al, 1994 for a full description of the two models and their results). Surface winds and wave information have been extracted at 0.5 degree interval for the whole Mediterranean Sea. They cover a full ten year period, from July 1992 till June 2002. The data are available at 6 hour interval, for the synoptic hours 00, 06, 12, 18 UTC.

During the ten year period we have considered (July 1992 – June 2002), the resolution of the meteorological model was changed twice. In 1998 ECMWF passed from T213 to T319, the number representing the truncation level in the two-dimensional Fourier series expansion used to describe the fields. Then, in November 2000, a major change was introduced with the shift to T511 (~40 km resolution. While the change from T213 to T319 did not cause large variations in the quality of the model results, the shift to T511 was a momentous event, that led to a substantial improvement of the results. Therefore it would not be correct to carry out a single calibration on the ten year data-set we have at disposal. The divide line is at 21 November 2000, when the model was moved to T511. Two separate and distinct calibrations have been carried out, for the period before and after this date.

The satellites considered as a reference for calibration are ERS1-2 and Topex. However, the previous assimilation of part of the satellite data in the meteorological and wave models precludes their use for the calibration of the model data. Therefore for the actual calibration we can make use of the following data:
wind speed, Topex and ERS1-2 altimeter data,
wave height, Topex altimeter data; ERS-1 altimeter data, i.e. till 1995; ERS-2 altimeter data, only for sufficiently large wave heights, and only till 1998.

CALIBRATION PROCEDURE

The model data have been extracted at 0.5 degree intervals, for both wind and waves, for the whole Mediterranean Sea. The data are available at the archiving six hour interval (four times a day). Hence from the ten year period, almost 15,000 data are available for each grid point.

As a rule the satellite data, taken along the ground track of the flight orbit, do not coincide with the positions (the grid points) and times (synoptic times at six hour interval) where the model data are available. Therefore for each satellite measurement, an interpolation in time and space has been done to derive the corresponding model estimate. This has led to a large data-set of corresponding couples of satellite-model data, distributed throughout the basin. Then each couple has been assigned to the closest grid point (with 0.5 degree resolution). For each grid point this has produced a set of couples, that could be used for the statistics, at that grid point, between model and satellite data. In particular we have evaluated for each grid point the best-fit slope between model and measured data, and their scatter around the best-fit. While the slope provides an estimate of the required local correction coefficients, the scatter is an indication of its reliability.

The different amount of data available at the various locations and the local orographic characteristics lead to a reliability of the results rather variable in space. Therefore, rather than considering the single calibration values at all the 0.5 degree grid points (about 950 of them), we have deemed more scientifically sound to consider only a reduced selected number of them (about 240), each summarising the information available in the surrounding area, in so reducing the uncertainty of the final results.

RESULTS AND DISCUSSION

Following the procedure described in the previous section, we have evaluated the correction coefficients for the chosen subset of Mediterranean grid points. The resulting maps, as isolines, for wind speed and wave height, are shown respectively in Figure 1 and Figure 2 for the period from July 1992 till November 2000. Note that the figures show the slope of the best-fit lines, which can be interpreted as the inverse of the correction coefficients required at each location.

Analysing the distribution of the isolines, it is immediately evident that their value grows moving from North to South. In other words the quality of the model results increase moving from the European toward the African coasts. This reflects the fact that most of the storms that affect the basin come from the North to North-West sector and the influence of land in the first few hundreds of kilometres off the coast. Besides the whole northern border of the Mediterranean Sea is characterised by a pronounced orography, that further affects the wind, hence the wave, fields. From the figures this is evident all along the Alboran Sea, the Western Mediterranean Sea, the Ligurian and Adriatic seas, the Aegean Sea and just south of Turkey. On the contrary the African storms, i.e. winds blowing from the Sahara, are relatively rare and in any case they are not affected, in Libya and Egypt, by a marked orography.

The calibration facors so obtained have been used to correct the original model data, providing a high quality time series for wind and waves in the Mediterranean Sea.
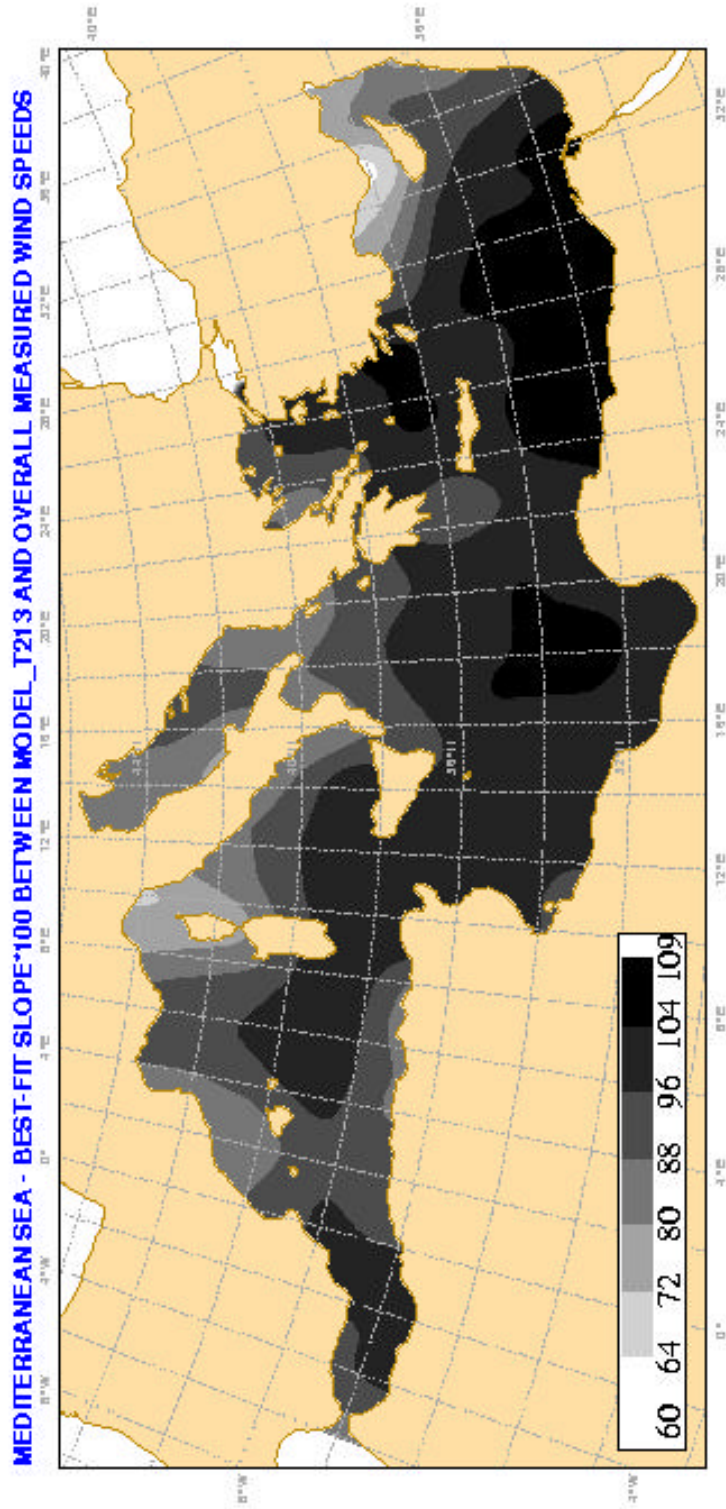
Figure 1 – Distribution of the best-fit slope between modelled and satellite measured wind speeds. Figures are slope*100. The period considered is before 21 November 2000.
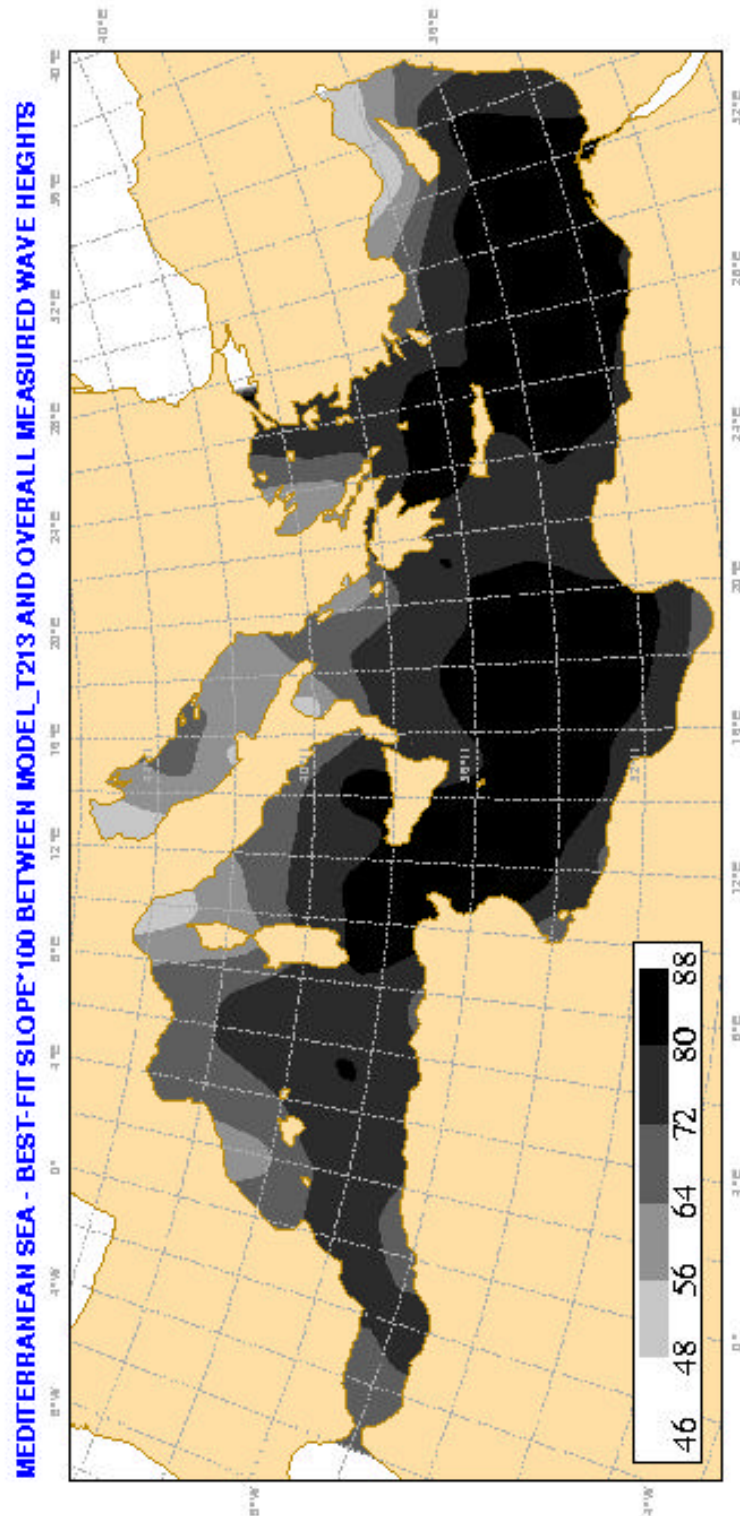
Figure 2 – Distribution of the best-fit slope between modelled and satellite measured wave heights. Figures are slope*100. The period considered is before 21 November 2000.

Ocean mixed layer response to a Bay of Bengal cyclone : A Case Study

A.A.Deo, D.W.Ganer and P.S.Salvekar
Indian Institute of Tropical Meteorology, Pune 411 008
E-mail : aad@tropmet.ernet.in

Introduction

Tropical cyclones are one of the most dangerous natural disasters that affect many countries around globe, cause tremendous loss of lives and property and severe disruption of socio-economic development. Indian subcontinent is worst affected by tropical cyclones in virtue of it's geographical positioning in the central part of the Indian Ocean and a long coastline spanning over 7500 km. A good knowledge of the ocean response to storm forcings is one of the key factors in tropical cyclone prediction. Various observational and numerical studies have shown that tropical cyclone produces significant changes in the underlying ocean thermodynamic structures which also involves SST changes. In the earlier studies the surface circulation and mixed layer depth variation in response to moving cyclones in the Indian Ocean has been studied considering idealized vortex and tracks by using 1½ layer reduced gravity ocean model.[1,2,3,4,9] . In the present study the case of 1994 cyclone is considered.

Numerical experiments and discussion of results

Experiment 1: The 1½ layer reduced gravity ocean model[9] used for this study, gives depth averaged currents, temperature and mixed layer depth. The cyclone TC02B (26 April to 3 May) of 1994 is chosen for this case study. The idealized symmetric cyclonic vortex of radius 400 km and maximum winds 20 m/s is allowed to move along the actual path of the cyclone (the track is shown in figure). The model is integrated for 7 days from an initial state of rest. The variations in the mixed layer depth and temperature are studied.

The model temperatures show cooling (warming) in the upwelling (downwelling) region. Figure 1(*a, b*) shows temperature change of mixed layer from the initial temperature of 29°C and mixed layer depth from the initial value of 50 m. The results indicate that the maximum cooling of about 4°C occurs little right of the track for day 5, which suggests that the mixed layer on the right of the track is cooled more than the left and there is right bias in the temperature field. The isotherms exhibit an oscillation with wavelength of ~600 km. The mixed layer depth field also has the right bias, the maximum upwelling is on the right of the storm track. The inertial wave in the wake of the cyclone has a wavelength of about 400 km. The surface circulation is also obtained which shows the divergence of the flow near the storm center. Also, the maximum magnitude of currents is located right of the storm track (figure not shown). These results are in agreement with the earlier studies. [2,5,6,7]

The model simulated temperature change is compared   with the OI SST change. It is found that the model produced cooling or warming is slightly overestimated than the observed SST change (figure1 *c,d*).

Experiment 2: In order to improve the results, another experiment is carried out. In this experiment the model response for the actual cyclonic wind data is investigated. The model is run for 10 years to reach the steady state using daily climatology of SSM/I winds obtained for the 3 years 1994 to 1996. The daily SSM/I surface winds data for the year 1994 is validated for the cyclonic vortex in the period of cyclonic storm. The cyclonic circulation is clearly visible of about 400 km radius for all the cyclone cases. The wind speed however, is less as compared to the real storms. In order to give real cyclone winds to the model as input, the idealized cyclonic vortex (bogus vortex) is superimposed on the real data[8]. The bogus cyclone winds are analytically generated by taking into account the real cyclone parameters such as size and intensity. This is considered as cyclonic wind input. The model is integrated beyond steady state using inter-annual forcing for 1994. Using the initial conditions of 25 April the model is integrated further for 7 days with superimposed cyclonic vortex.

The figure 1 *e* and *f* shows the model temperature field obtained by taking the differences of with & without cyclone case, for 5th day and for the experiment 1 discussed above. Comparing the model temperatures in both the experiments, it is seen that the magnitudes are reduced by about 1°C for the experiment 2, when compared with the experiment 1. Therefore, the model temperature change in the superimposed case is close to the observed temperature change during the passage of the cyclone. Other features such as right bias, lag between maximum cooling and storm position etc., do not change significantly.

References:

Behera S.K, Deo A.A, and Salvekar P.S., 1998: Investigation of mixed layer response to Bay of Bengal cyclone using a simple ocean model. Meteorol. Atmos. Phys.,65, 77-91.

Chang S.W. & Anthes R.A., 1978: Numerical simulation of the ocean's nonlinear baroclinic response to translating hurricanes. J. Phys. Oceano., 13, 468-480

Deo A.A, Salvekar P.S and Behera S.K,2001a: Oceanic response to cyclone moving in different directions over Indian Seas using IRG model. Mausam, 52, 163-174.

Deo A.A,Ganer, D.W.,& Salvekar P.S,2001b: Upper ocean response to a moving cyclone in south Indian Ocean. WGNE Report on Research Activities in Atmospheric and Ocean Modelling,, pp 8.3-8.4

Graetbatch R. J., 1983,:On the response of the ocean to a moving storm: The nonlinear dynamics. J. Phys.Oceano., 13, 357-367

Price J.F., 1981: Upper ocean response to a hurricane. J. Phys. Oceano., 11,153-175.

Price J.F., 1983: Internal wave wake of a moving storm: Part 1, Scales energy budget and observations, J. Phys.Oceano., 13(6), 949-965.

Thu T.V.& Krishnamurti, T.N., 1992: Vortex initialization for typhoon track prediction. Meteor. Atmos. Phys., 47, 117-126.

A.A.Deo, D.W.Ganer and P.S.Salvekar, 2002:Ocean mixed layer response to the tropical cyclone moving in different directions in the south Indian Ocean WGNE Report on Research Activities in Atmospheric and Ocean Modelling,, pp 8.1-8.2
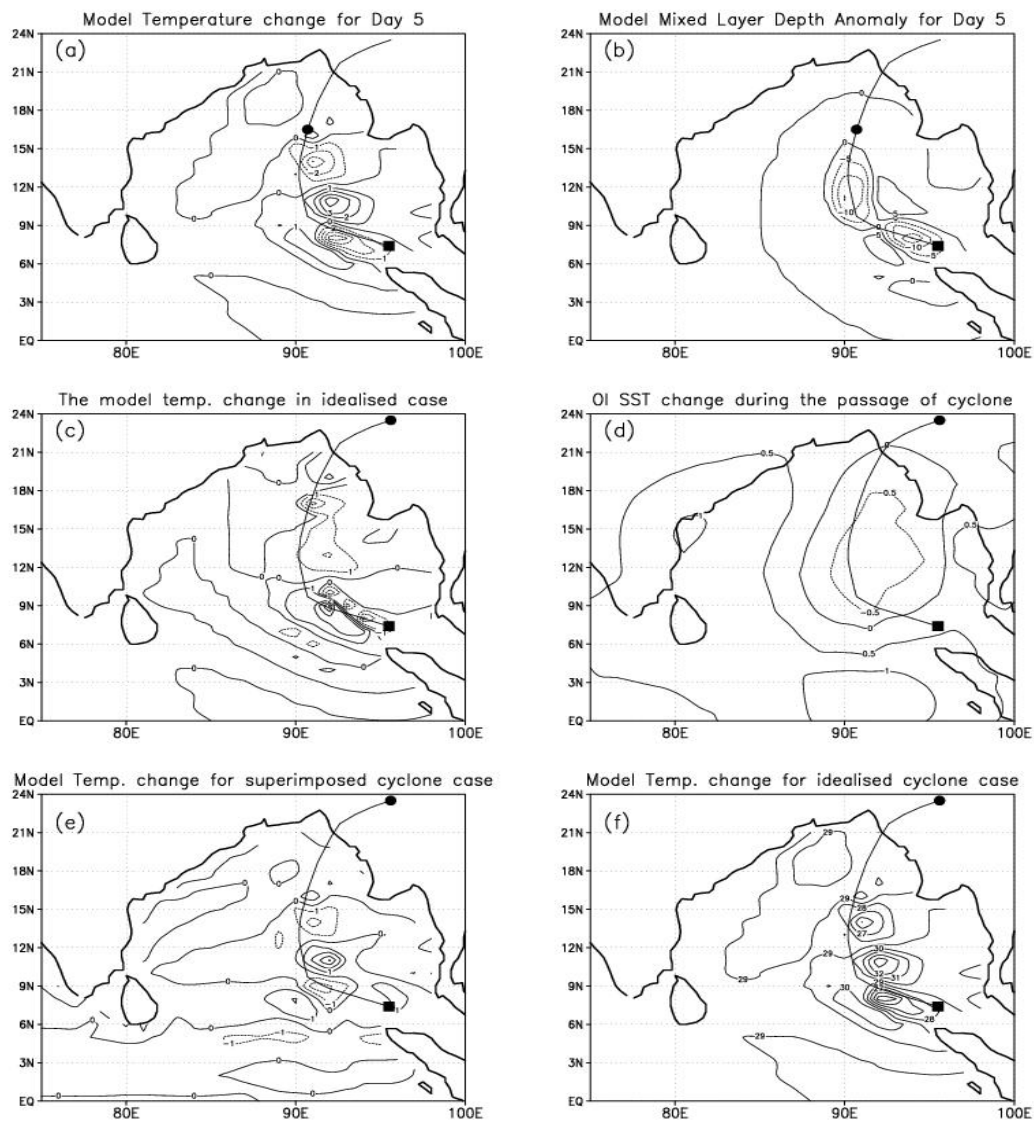
Fig1 : Model mixed layer depth anomaly and temperature change compared with
observed SST change and temp. change in superimposed cyclone case.
Solid line indicates the storm track.

Ocean Data Assimilation Using Temperature, Salinity, and Sea Surface Height Observations, and Its Impacts on El Niño Prediction

Masayoshi Ishii*, Kenji Sakamoto**, and Masahide Kimoto***

* Climate Prediction Division, Japan Meteorological Agency; ishii@naps.kishou.go.jp
** Climate Prediction Division, Japan Meteorological Agency; k-sakamoto@met.kishou.go.jp
*** Center for Climate System Research, University of Tokyo; kimoto@ccsr.u-tokyo.ac.jp

A three-dimensional variational ocean data assimilation system using temperature, salinity, and sea surface height (SSH) observations was developed, and the impacts of the data assimilation on El Nño prediction by a coupled ocean-atmosphere model was studied.

In ocean model integration without data assimilation, atmospheric forcing plays essential roles in reproducing seasonal and interannual variations, but it also causes sizable biases in temperature and salinity fields. By data assimilation, these biases are significantly reduced and the intraseasonal variations appear to be well reproduced. In case of salinity assimilation, its outputs have been verified using TRITON-buoy observation. Introduction of SSH observation to data assimilation makes variability of model temperature and salinity larger by a factor of 1.5−2.0 in data sparse regions, e.g., the Indian and equatorial Atlantic Oceans, than a case without SSH data assimilation.

El Niño prediction experiments were carried out using several types of ocean initial condition; temperature (T) and salinity (S) assimilation (TSAS), T, S, and SSH assimilation (TSHAS), and T assimilation with/without climatological salinity constraint (TAS+Sclim/TAS+Sfree). Figure 1 shows anomaly correlation skill (ACC; %; upper) and root-mean-square error skill (RMSE; ˚C; bottom) with a function of lead time (days) for Niño-3.4 sea surface temperature (SST) anomalies predicted from 83 initials in 1993 − 1999. Large differences in skill are found between prediction with TAS+Sfree (dashed) and the others. Initially, salinity of TAS+Sfree is far different from climatology and the errors of predicted SSTs grow rapidly rather than those of the other predictions. Small improvement of prediction skill using TSAS and TSHAS initials may be owing to sparseness of salinity observation and incompleteness of an SSH assimilation scheme adopted in the system, although further investigations are necessary.

Fig. 1.

In future, the system will be equipped with a current update scheme by which model currents are adjusted to updated density fields, as well as an revised dynamical model and improved data assimilation schemes. In addition, data impacts on El Niño prediction will be reexamined.
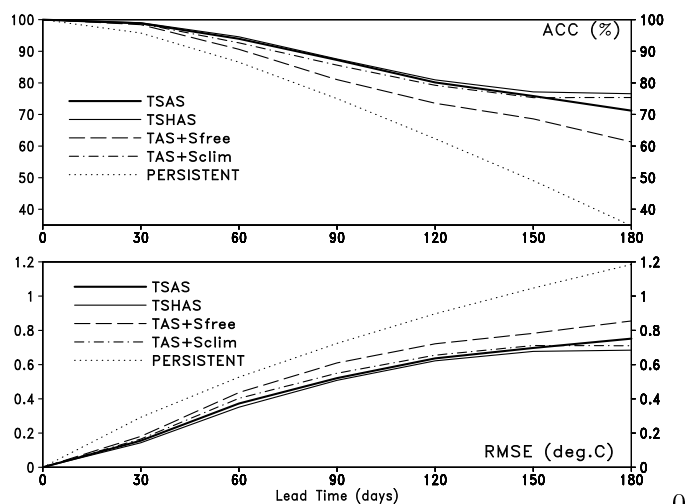
Modeling frontal instabilities in the Gulf of Mexico

Erik Kvaleberg[1], Steven L. Morey and James J. O'Brien
The Center for Ocean-Atmospheric Prediction Studies
The Florida State University

Satellite images of sea surface temperature (SST) and chlorophyll in the eastern Gulf of Mexico show filaments of relatively cold water extending from the coastal zone out towards the shelf break. Similar structures have been observed in the California Current system (Ikeda & Emery, 1984) and Portugal (Røed & Shi, 1999), and have been linked to both upwelling and topography irregularities along the coast.

Fig. 1. Satellite image showing chlorophyll distribution on the west Florida shelf.

In this study the Navy Coastal Ocean Model (NCOM) (Martin, 1999; Morey et al, 2003) is used to investigate filaments on the west Florida shelf. The domain is a square basin with a 320 km long coastline at the eastern boundary. There are 40 vertical layers; the upper 20 are sigma levels while the bottom 20 (below 140m) are z-levels. The model is set up with idealized shelf topography uniform in the north-south direction, with a minimum (maximum) depth of 4m (1500m). The mixed layer has an initial temperature of 22°C and maximum thickness of 140m at the shelf break, 200 km from the coast. Further down, the temperature decreases linearly toward the bottom. Periodic boundary conditions are used to the north and south, and at the western boundary the model uses Orlanski radiation. The only forcing of the system is uniform surface cooling of 70 Wm^{-2}.

Starting from rest, a thermal front is almost immediately formed in the shallow water close to land (within 1-2 days). As time progresses, the density difference becomes large enough to set up an equatorward current along the coastline, which seems to become unstable after approximately 6-8 days. Small undulations rapidly grow to meanders of 40 km or more, and eddies begin to form and propagate westward, dissipating 60-80 km from the coast. The filaments have a separation distance of 20-30 km (Fig. 1 a, b).

---

[1] erik@coaps.fsu.edu

A suite of experiments with varying parameters are being used to explain the dynamics of the cold filaments. A steady growth of the initial undulations in the density current, along with nearly vertical isotherms, indicates the presence of baroclinic instability, however these issues require further study.
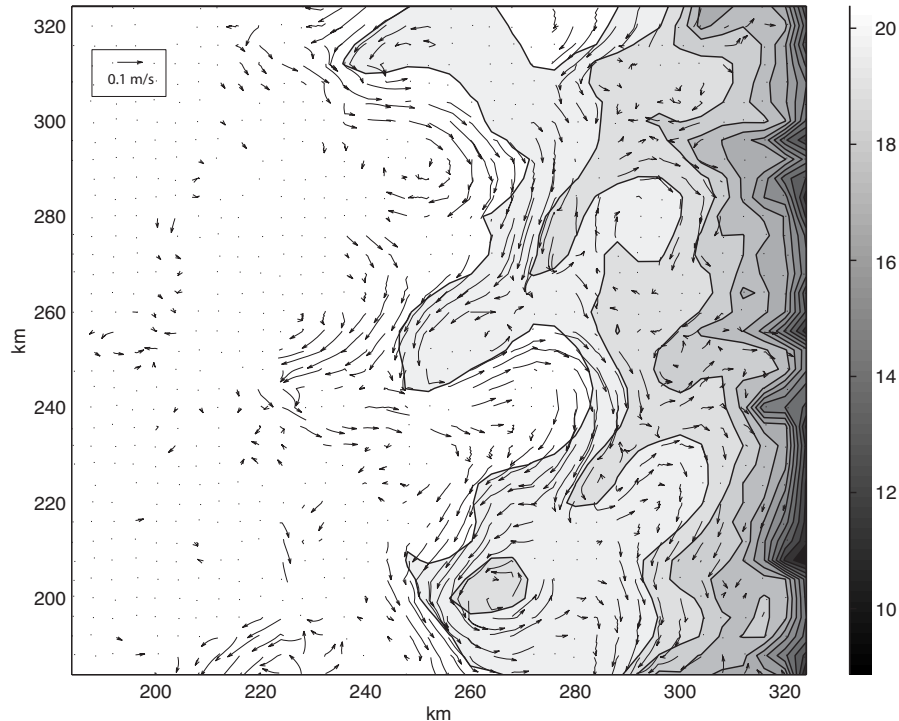

Fig 2. Modeled SST (contours) and surface currents (vectors) at day 60.

References:

- Ikeda, M. and W. J. Emery, Satellite observations and modeling of meanders in the California current system off Oregon and northern California, J. Phys. Oceanogr., 14, 1434-1450, 1984.
- Martin, P. J., A description of the Navy Coastal Ocean Model Version 1.0, NRL Report: NRL/FR/7322-009962, Naval Research Laboratory, Stennis Space Center, MS, 39 pp. 2000.
- Morey, S. L., P. J. Martin, J. J. O'Brien, A. A. Wallcraft and J. Zavala-Hidalgo, Export pathways for river discharged fresh water in the northern Gulf of Mexico, J. Geophys. Res., In review, 2003.
- Røed, L. P. and X. B. Shi, A numerical study of the dynamics and energetics of cool filaments, jets, and eddies off the Iberian Peninsula, J. Geophys. Res., 104, C12, 29817-29841, 1999.

NUMERICAL INVESTIGATION OF DIFFERENT TYPES OF OPEN BOUNDARY CONDITIONS BY MODELLING OF THE INTERNAL-WAVE TRANSFORMATION AT THE EDGE OF THE SHELF BY M2 TIDAL FORCING

Arkadiy S. Safray and Igor V. Tkatchenko*

P.P.Shirshov Institute of Oceanology, Russian Academy of Sciences,
St. Petersburg Branch, 30, 1-st Linia V.O., 199053, St. Petersburg,
RUSSIA

*Corresponding author. E-mail: tkat@gk3103.spb.edu

To investigate the problem, (see the title) the 3-D rigid-lid model of marginal sea has been used. The model includes non-hydrostatic system of primitive equations of motion, equations of continuity, temperature, salinity, and constructed from them 3-D Poisson equation for pressure and is completed with the equation of state and k-ε closure of Kantha and Clayson (1994) type. Numerical approximation of the equations of the model is based on tetrahedron finite element and has the 2nd order of accuracy in time and space both. Near the shelf zone the nest grid was thickened up to 4 m in the horizontal and 1 m in the vertical direction. Angle of the shelf plateau declination is 80°.

Flather (1976) and Orlanski (1976) radiation conditions for velocity vector (V), temperature (t) and salinity (s) at the outflow as well as periodical ones were tested. To avoid a loss of mass, radiation conditions are rather of modified Perkins et al. (1997) type.

All experiments were initialized from $V=0$ and designated vertical profile of s and t typical for northern shallow regions of the ocean all over the domain.

Here we present some results at z-x central cross-section of numerical solutions for experiments with radiation conditions for t and s and periodical (left column) and Flather radiation boundary conditions (right column) for V for the moments 8.25T and 8.5T (T - M2 period).

It is seen that the speed of propagation of the internal wave is greater and its front is much more expressed by the periodical boundary conditions for the both open sides of the domain, but propagation of the salinity through the left boundary is limited in contrary with the experiment with radiation boundary conditions at this boundary for the first half of the M2 period. (U-component is directed to the left). Flux of the salinity to the near shore region is too small and radiation boundary conditions seem more preferable.

The comparison of the Available Potential Energy (APE) and the Turbulent Kinetic Energy (TKE) illustrations with illustrations for salinity allows detection of the internal wave destruction zones. Regions where APE and TKE both have its maximum values coincide with zones of subcritical angles of isopycnes.
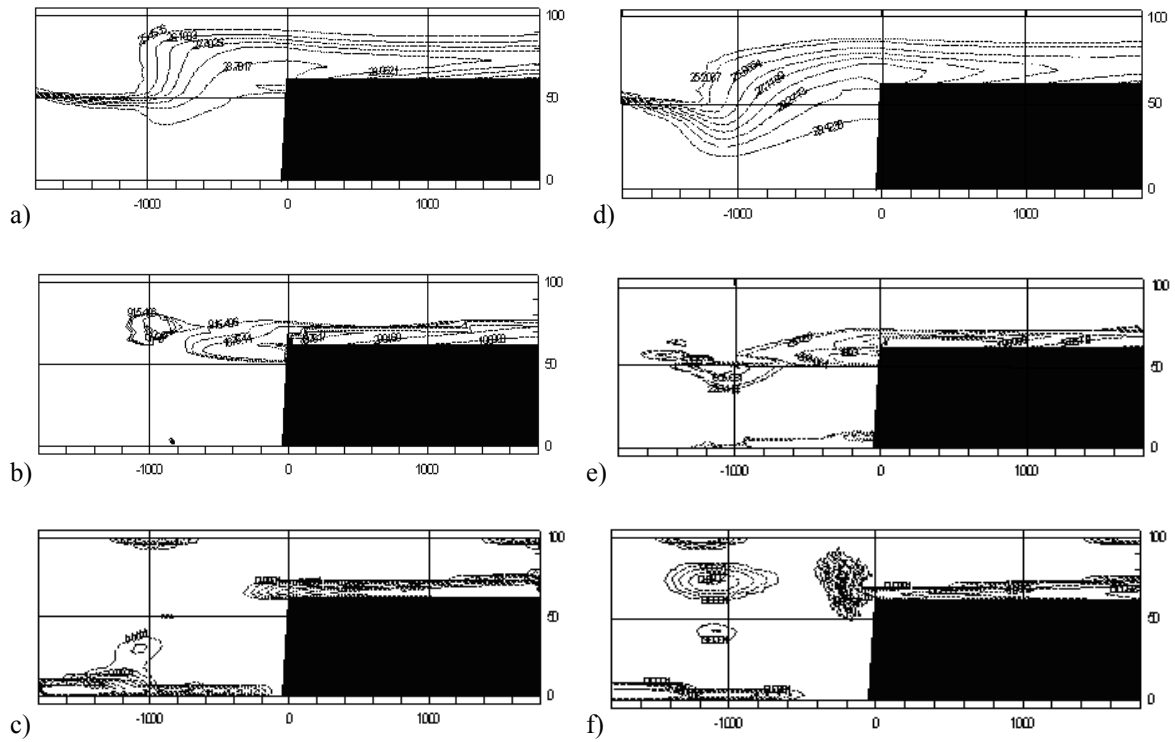
Figure 1. Central *z-x* cross-section of the salinity, APE and TKE fields at 8¼ T: (a), (b), (c) – periodical boundary conditions; (d), (e), (f) – Flather' boundary conditions. (*z, x* in meters).

Figure 2. Central *z-x* cross-section of the salinity, APE and TKE fields at 8½ T: (a), (b), (c) – periodical boundary conditions; (d), (e), (f) – Flather' boundary conditions. (*z, x* in meters).
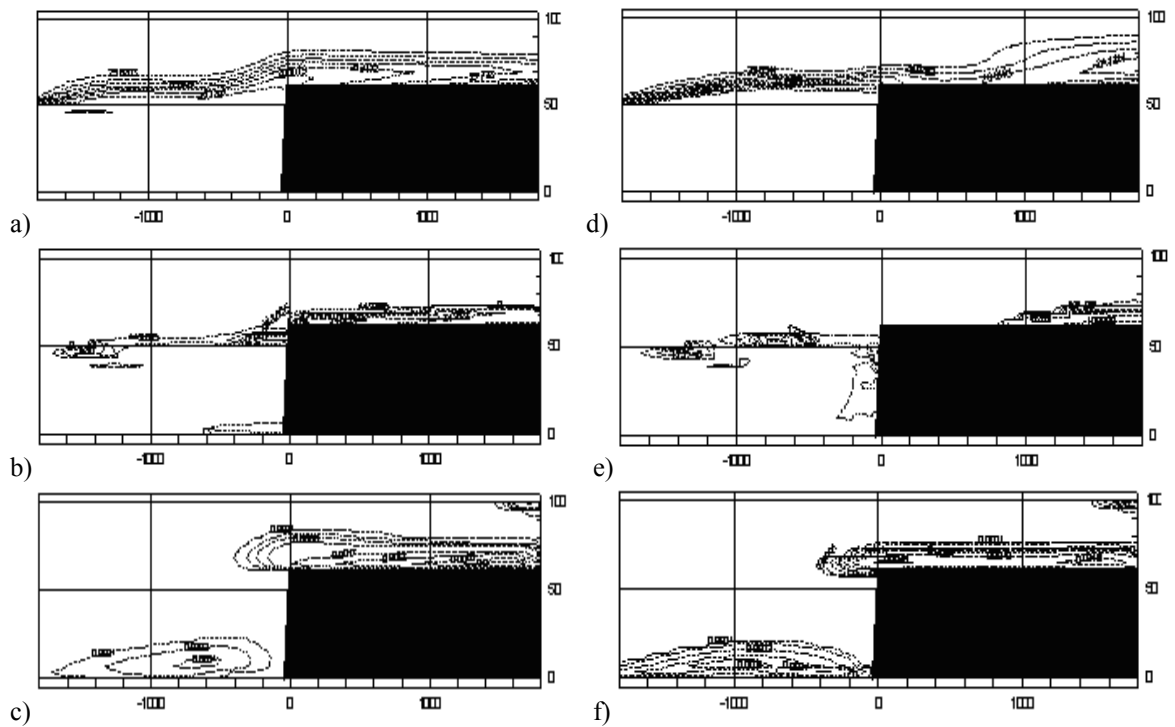
Fifty years Time-integration of Global Eddy-resolving Simulation

Hideharu Sasaki[1], Nobumasa Komori[1], Keiko Takahashi[1], Yukio Masumoto[2,3], Hirohumi Sakuma[1]

1: *Earth Simulator Center, Yokohama, Japan*   2: *Frontier Research System for Global Change, Yokohama, Japan*

3: *Grad. Schl. of Science, Univ. of Tokyo, Tokyo, Japan*

E-mail: sasaki@es.jamstec.go.jp

1. Introduction

The key elements that determine the basic properties of the general circulations of the world ocean are nonlinear scale interactions between mesoscale eddies and basin scale circulations.   The Earth Simulator enables us to perform eddy-resolving simulations on the global domain to assess simulated eddy-dynamics together with the phenomenological validations of our numerical experiments.   In order to pursue this goal, we have developed a high-resolution MOM3-based OGCM code (OFES) optimized for the Earth Simulator.   We have executed a fifty-year time integration of the global eddy simulation.

2. Model setting and tuning

The computational domain covers a near-global region extending from 75° S to 75° N.   The horizontal resolution and the number of vertical levels we employed are 0.1 degree and 54 respectively.   The model was spun up from annual mean temperature and salinity fields (WOA98) without motion.   The surface fluxes are specified from monthly mean NCEP re-analyses data in addition to a surface salinity restoring to climatological value.   To suppress grid-scale noises, we introduced a scale-selective damping of Bi-harmonic type and employed KPP scheme for the vertical mixing.

To attain high performance of our eddy resolving code, a number of different optimization techniques have been utilized considering distinctive characteristics of the Earth Simulator.   After intensive vectorization of the code, we have done an optimal parallelization taking the characteristics of inter- and intra-node communications into account.   The computational domain on the sphere is divided into zonal strips bounded by four latitude circles and the number of PE employed is 1500 (188 nodes).   The parallel efficiency and vector ratio of our code are 99.52% and 99.87% respectively and one model-year simulation has been completed in seven hours.

3. Results

Simulated annual mean sea surface height distribution is shown in Figure 1.   We can clearly see that, in consistent with a simple geostrophic relation, the SSH in the subtropics is higher than that in the sub-polar region and the lowest SSH appears in the southern flank of the strong Antarctic Circumpolar Current.   A zonal band of lower SSH can be noticed along 7°N in the Pacific, which corresponds to the boundary between the North Equatorial Current and the North Equatorial Countercurrent.   Therefore, we can say that the basin-wide pattern of the mean SSH field is simulated well.

Smith et al. (2000) suggest that the distribution of eddy activity becomes realistic compare to that derived observation data with increasing horizontal grid spacing.   Fig.2 shows the root-mean-square variation of the simulated SSH anomaly.   The variability maxima appear in the western boundary current regions such as the Kuroshio/Kuroshio Extension, the Gulf Stream/the North Atlantic Current, the Malvinas Current and the Agulhas Current and around the Antarctic Circumpolar Current.   Fairly high variability regions are also seen along 20N and 6N in the western Pacific.   Locations of these high variability regions are observationally confirmed by the satellite altimetry (Le Traon and Orgor, 1988).

The snapshot of the sea surface height and the velocity field (Fig.3) suggests that the model reproduces the several eddies, so-called Agulhas Rings shed at the Agulhas retroflection.   The scale of the simulated Agulhas Rings is close to the observation.   The high resolution of the model contributes to resolve mesoscale eddies.
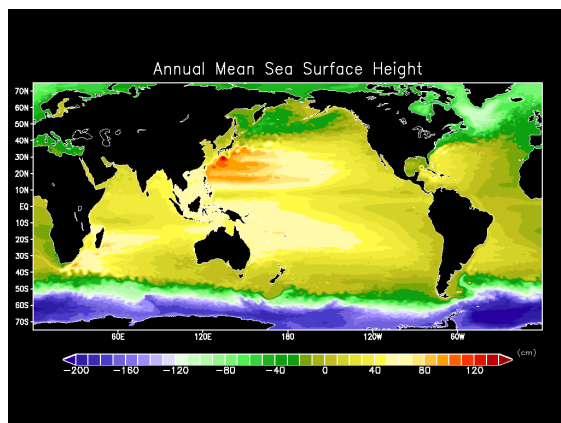
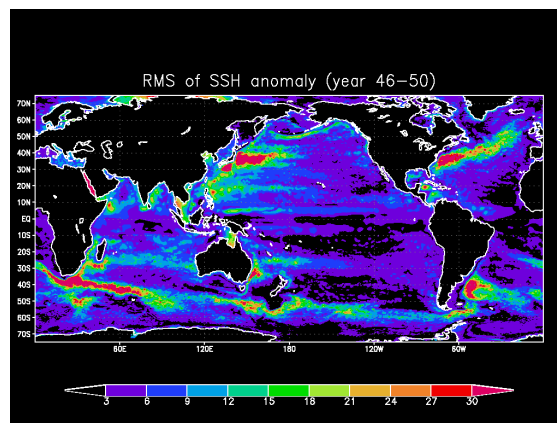Fig.1 Simulated annual mean sea surface height.

Fig.2 Root-mean-square variation of sea surface height.

It is well known that in low-resolution simulations the Kuroshio tends to overshoot to the north and the resulting separation point turns out to be quite unrealistic. The composite of the simulated monthly mean Kuroshio paths during the year 46 is shown in Fig.4. The Kuroshio separates with right latitude and the Kuroshio Extension bifurcates into two branches. Observation (Mizuno and White, 1983) suggested that the bifurcated Kuroshio Extension is controlled by the bottom topography.
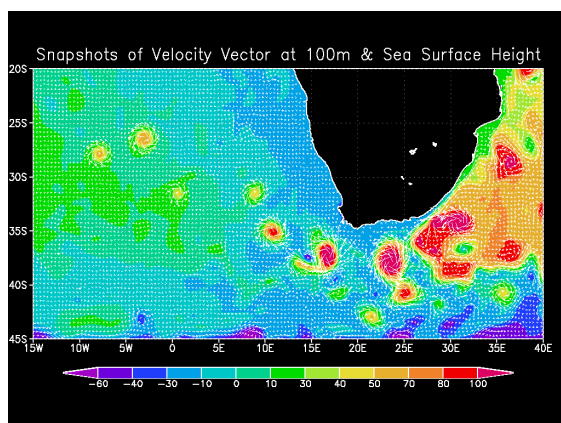

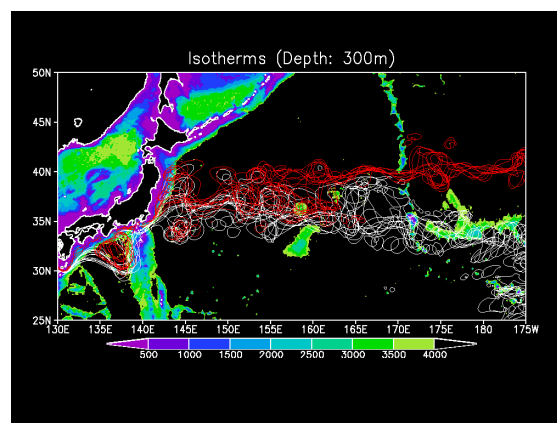Fig.3 Snapshot of sea surface height and velocity velocity vector at 100m.

Fig.4 Monthly-mean Kuroshio Current paths as defined by the 14 (Black) and 10 (red) isotherm at 300m depth, superimposed upon bathymetry.

4. Summary

A quick look at the simulated result tells that the overall characteristics of oceanic fields are quite realistic. The hi-resolution of the model contributes to resolve the fine structure such as the mesoscale eddies, which encourages us to extend our investigation further on variety of topics.

Reference

Le Traon, P.-Y. and F. Ogor, 1998: ERS-1/2 orbit improvement using TOPEX/POSEIDON: The 2cm challenge, *J. Geophys Res.*, 103, 8045-8057.

Mizuno, K., and W. B. White, 1983: Annual and interannual variability in the Kuroshio current system. *J. Phys. Oceanogr.*, 13, 1847-1867.

Smith, R. D., M. E. Maltrud, F. O. Bryan, and M. W. Hecht, Numerical simulation of the North Atlantic Ocean at 1/10, *J. Phys. Oceanogr.*, 30, 1532-1561, 2000.

Estimation of Heat Transports in the Indian Ocean using Altimetry and MICOM

Bulusu Subrahmanyam and James J. O'Brien
Center for Ocean Atmospheric Prediction Studies (COAPS),Florida State University, Tallahassee, USA
Vijaykumar Manghnani
Weather Predict LLC, Raleigh, USA.
Lian Xie and John M. Morrison
Department of Marine, Earth and Atmospheric Sciences, North Carolina State University, Raleigh, USA.

We have developed a new technique to estimate the heat budget of the Indian Ocean using TOPEX/Poseidon (T/P) Sea Level Anomalies (SLA) and the Miami Isopycnal Coordinate Ocean Model (MICOM) in order to study the redistribution of heat in the Indian Ocean

Satellite altimetry with its abundant spatio-temporal coverage of the ocean provides an excellent opportunity to study the heat propagation in the ocean. These observations can be used for validating model results and also for improving models. Of particular interest to this study is the heat content redistribution over the Indian Ocean. The heat content anomalies of the ocean have been estimated from T/P Sea Level Anomalies (SLA), based on the assumption of a linear relation between sea-level change and the heat content of the water column. In regions of strong variability in the upper ocean heat content, such as the Indian Ocean, the derived heat content anomalies provide useful tools to study the spatial and temporal variability.

Heat Transports from altimetry

The sea level change due to heating can be approximated from the sea level anomaly measured by the altimeter (Manghnani et al., 2002) as:

$$\Delta\eta = \Delta\eta^{TOPEX} + \in \qquad (1)$$

where $\in$ is the error introduced by neglecting salinity and barotropic effects, as well as errors in altimetric measurement. Chambers *et al*. (1997) conclude that the size of $\in$ is at most 1 - 2 cm for the annual amplitude over most of the ocean. As we have seen, it may be ~ 6 cm in the Bay of Bengal.

Monthly surface flux data for net radiation (R_{sfc}) for 1993 - 1996 were obtained from the NCEP/NCAR) re-analysis. The latent heat flux (LHF) and sensible heat flux (SHF) were derived from the model simulations, as described in the model section. These data were used to calculate the net oceanic heat gain (Q_{sfc}) from the atmosphere, using the relation

$$Q_{sfc} = R_{sfc} - LHF - SHF \qquad (2)$$

The net oceanic heat gain used for application with the model and T/P derived fields is calculated using the same datasets.

The monthly heat storage anomalies were estimated using centered time differencing of the heat content anomalies. The value of heat storage thus obtained was subtracted from the net oceanic heat gain to yield an estimate of the oceanic heat flux divergence.

Heat transports from MICOM:

The Miami Isopycnic Coordinate Model (MICOM) is used in this study. MICOM is a three-dimensional primitive equation ocean general circulation model (OGCM) with 15-isopycnic layers and a mixed layer on top. The model is run in global configuration. A major modification is the implementation of a variable resolution horizontal grid, which is designed such that the resolution gradually increases while approaching the East African coast, the Indian subcontinent and the Indonesian Through flow (ITF) region (Fig. 1). The grid is generated by conformal mapping the North and South Poles to arbitrary locations on the Earth, in this case to one location near the coast of Africa (5°N, 38°E) and the other in one of the islands of Indonesia (0°N, 110°E).

The resulting grid has enhanced resolution in the Indian Ocean region and is inherently orthogonal. For this application we have chosen a grid which maintains relatively high (20-60 km) resolution in the northern Indian Ocean model domain to represent the transport by major current systems, equatorial phenomenon and the ITF.

The model was spun up from rest, using climatological forcing from the Climatology COADS for 6 years, by which time the top seven layers (*ie*. a depth of ~ 500m) of the model ocean had reached quasi-steady state. The model was then forced by monthly wind stress, radiation, wind speed, specific humidity and air temperature from the NCEP/NCAR reanalysis project for the 20-year period from January 1980 to December 1999. The model latent and sensible heat fluxes were calculated using wind speed dependent heat transfer coefficients. These fluxes are used along with the radiation fields to calculate the net oceanic heat gain using equation (2). Since most of the variability on seasonal to inter-annual scales is in the top 500 m of the Ocean, the model heat content is derived by integrating the top seven layers. The monthly heat storage was estimated as the rate of change of heat content using a 2nd order centered time difference scheme. Finally, the heat storage was subtracted from the model surface heat flux to yield the upper ocean heat flux divergence.

Fig. 2 shows the comparison between MICOM and altimetry of the annual march of the integrated variability in the region. The northern Indian Ocean experiences the most dramatic changes in its heat content over the annual cycle. Integrating the surface flux, the heat stored and the heat transport for the region north of the Equator, further condenses the variability in this region. During the winter, the north Indian Ocean gains heat, corresponding with northward transport of heat across the equator. During the summer, despite a net input of surface heat flux, there is a depletion of heat from the upper ocean. This is matched by an almost equal amount of heat transport south of the Equator. These patterns are clearly depicted even though the T/P derived estimates are weaker.
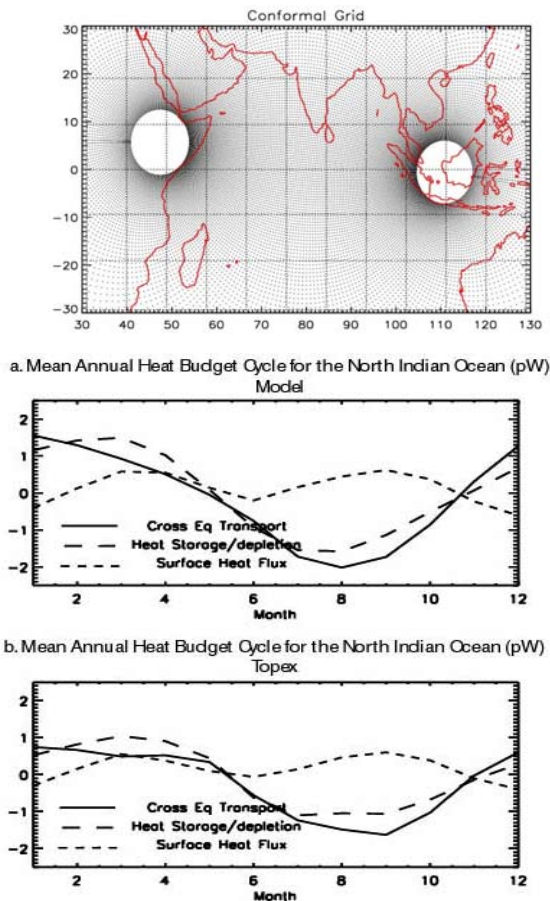

Figure 1. The global varying resolution grid used in the MICOM Indian Ocean Model. Only the Indian Ocean portion is shown. The poles are placed over land and thus avoiding the singularity problem. The resolution varies from 0.2° - 0.5° in the northern Indian Ocean and 0.5°-1° in nearby basins.

Figure 2. The mean annual cycle of the heat budget terms in the North Indian Ocean for (a) model derived fields and (b) the T/P SLA derived fields. The net oceanic heat gain, heat storage and heat transport are integrated over the northern Indian Ocean.

Improvement of wind induced mixing and entrainment in MRI mixed layer model

Akiyoshi WADA

Meteorological Research Institute, Tsukuba, Ibaraki, Japan

1. Introduction

The interface between the atmosphere and the ocean is known as an active boundary where surface heat fluxes and wind stresses are exchanged. The atmospheric forcing is also responsible for complicated dynamics and thermodynamics in an oceanic mixed layer. These dynamics and thermodynamics are associated with variations of sea surface temperature (SST). On the other hand, SST plays a key role in atmospheric phenomena because turbulent heat fluxes like sensible and latent heat flux are closely related to SST. To develop an atmosphere-ocean coupled model for a short-term forecast such as predictions of tropical cyclones, a mixed layer model, which is an oceanic part of typhoon-ocean coupled model, has been developed at the Meteorological Research Institute (MRI) in Japan Meteorological Agency (JMA). According to Wada (2002), the mixed layer model has turbulent mixing processes such as stabilizing buoyancy fluxes, wind-induced mixing, and vertical shear mixing near the surface in imitation of Price et al. (1986) and entrainment at the bottom of the mixed layer by parameterization of Deardorff (1983). In the present work, both the near-surface process and entrainment parameterization are modified. Observed SSTs by R/V Keifu-Maru are used to validate simulated SSTs by mixed layer model. It is noted that atmospheric forcing to the ocean (wind stresses and heat fluxes) used in the present work are estimated by empirical formulas such as Kondo (1975), Reed (1977), and so on.

2. Modification of MRI mixed later model

Two turbulent mixing processes are modified from previous MRI mixed layer model (Wada 2002). One modification is to reconstruct vertical mixing near the surface. Because Stokes drift is dominant near the surface, vertical shear mixing near the surface can be neglected. In contrast, the process of wind-induced mixing is re-programmed over in order that seawater near the surface may be stirred well even under the moderate wind velocity. On the occasion of this modification, SST depth is defined of 1m instead of 2.5m employed by Wada (2002). The other revision is relevant to a part of entrainment processes at the bottom of the mixed layer. According to Deardorff (1983), entrainment rates are determined by combination of the Richardson

number of frictional velocity, buoyancy fluxes, and vertical shear. The vertical shear is estimated by equations of motion in MRI mixed layer model. Here, the criterion of the Richardson number related to vertical shear at the bottom of the mixed layer (we call it the gradient Richardson number) is excluded and background Richardson number at the regions where there is extremely small vertical shear at the bottom of the mixed layer is assumed to be 2.5.

3. Experiments and results

By doing these modifications, computed SSTs under less than 5m/s at 3°N,137°E on November 1994 and nearly 10m/s wind velocity at 20°N, 130°E on August 1998 is simulated better than those of previous model. Fig.1 represents the observed SSTs and computed SSTs at 3°N,137°E on November 1994 under the assumption that the gradient Richardson number is uniformly set to 0.83 during the integration. Maritime observed SSTs, sea temperatures below the surface and salinity throughout layers by conductivity, temperature, and depth measurements (CTD) are used as the oceanic initial condition. In this case, observed SSTs by CTD are almost the same as maritime SSTs. The variance and amplitude of diurnal cycling of observed SSTs are properly simulated in computed SSTs under less than 5m/s wind velocity. Solar radiation in the daytime and entrainment at the bottom of the mixed layer at night is significant for SST variations. Fig.2 represents the result of numerical experiment at 20°N,130°E on November 1994. The setting of oceanic initial condition is similar to the preceding procedure although observed SSTs by CTD are nearly 0.4℃ lower than maritime SSTs. However the gradient Richardson number is determined from data of ocean currents every 24 hours by acoustic current meter (ACM)
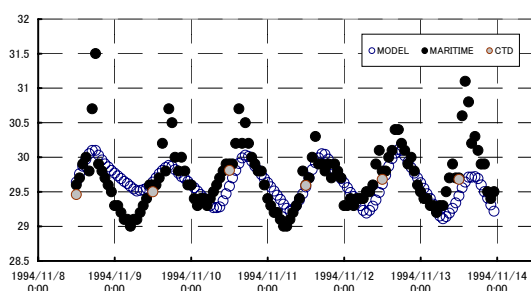

Fig.1 SST variations around 137°E and 3°N under less than 5m/s wind velocity on November, 1994. Close circle represents observed SSTs (●), open circle computed SSTs(○),and gray circle SSTs by conductivity, temperature, and depth measurements (CTD).

*Corresponding author address: Akiyoshi Wada, Meteorological Research Institute, 1-1 Nagamine, Tsukuba, Ibaraki 305-0052 Japan: email: awada@mri-jma.go.jp

equipped with R/V Keifu-Maru. The processes of wind-induced mixing and entrainment are effective for SST variations at night and suppressing the amplitude of diurnal cycling in the daytime
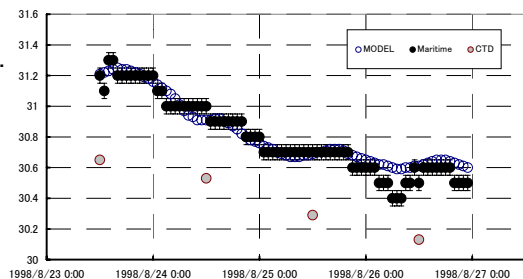

Fig.2 SST variations around 130° E and 20° N under less than 5m/s wind velocity on November, 1994. Close circle represents observed SSTs (●), open circle computed SSTs(○),and gray circle SSTs by conductivity, temperature, and depth measurements (CTD).
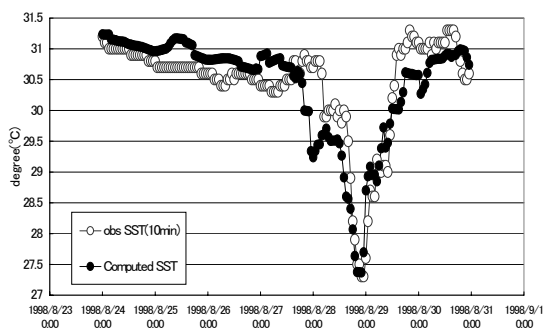

Fig. 3 Time series of maritime observed SSTs (○:open circle) and computed SSTs by upgraded mixed layer model (■:Close square) during August 24, 1998 to August 31, 1998

Observed SST cooling after the passage of Typhoon REX, which is nearly 3℃ decrease at 22JST in August 28 1998, is well simulated in comparison with the result of the previous report by Wada (2002) (Fig.3). The numerical experiments are conducted with global analysis data every 6 hours in JMA and Rankin vortex based on JMA best track maximum wind velocity corresponded to 10-minute average, not on Joint Typhoon Warning Center best track maximum wind velocity corresponded to 1-minute average. TRMM/TMI SSTs and climatological sea temperatures below the surface and salinity throughout layers are used as the oceanic initial condition. The result shown in Fig.3 suggests that maximum wind velocity averaged in 10-minute is appropriate for simulating SST variations. Even in this case, entrainment by the gradient Richardson number is crucial for SST simulation. At that time, the gradient Richardson number by vertical shear at the bottom of the mixed layer is mainly

determined from near-inertial currents after the passage of typhoons.

4. Discussion

Under the situation not only strong wind such as typhoons but also moderate or weak wind, we successfully simulate observed SST variations. Through the numerical simulations for SST variations under various wind conditions, we confirm that entrainment by the gradient Richardson number is commonly crucial for SST variations. Two approaches are attempted in setting the gradient Richardson number. As the first approach, SST variations shown in Fig.1 are simulated with the assumption that the gradient Richardson number is assumed to be uniformly 0.83. In contrast, as the second approach, SST variations shown in Fig.3 are simulated using the gradient Richardson number determined by 3-dimensional mixed layer model. Both approaches cannot help but be skeptical about the accuracy of the gradient Richardson number. In fact, the gradient Richardson number by vertical current shear includes near-inertial and geostrophic components. In the region around 137° E and 3° N, Equatorial Counter current may be dominant for vertical shear at the bottom of the mixed layer because in the first experiment, wind-induced currents are considered to be weak under less than 5m/s wind velocity. In contrast, wind-induced near-inertial currents are dominant after the passage of Typhoon REX. Under the situation that stationary currents are weak, the atmospheric forcing is important not only for near-inertial currents near the surface but also for vertical shear at the bottom of the mixed layer. If we need the SST variation more accurately, we will need a high-resolution 3-dimensional ocean model to estimate the vertical shear at the bottom of the mixed layer more accurate. Nevertheless this mixed layer model is able to endure in SST simulations over a period of a week.

References
Deardorff, J. W. (1983): A multi-limit layer entrainment formulation. *J. Phys. Oceanogr.,* **13,** 988-1002.
Kondo, J (1975): Air-sea bulk transfer coefficients in diabetic conditions. *Boundary Layer Meteorol.*, **9,** 91-112.
Price, J. F., Weller, R. A., and R. Pinkel (1986): Diurnal cycling: observations and models of the upper ocean response to diurnal heating, cooling, and wind mixing. *J. Geophys. Res.,* **91,** 8411-8427.
Reed, R. K. (1977): On estimating insolation over the ocean. *J. Phys. Oceanogr.,* **7,** 482-485.
Wada, A. (2002): Improvement of SST prediction by diurnal cycling algorithm in the MRI mixed layer ocean model. *CAS/JSC WGNE Research Activities in Atmospheric and Oceanic Modelling.* 08-29

A new gridding method for satellite altimeter data

Peng Yu[1], Jorge Zavala-Hidalgo, and James J. O'Brien
Center for Ocean-Atmospheric Prediction Studies, The Florida State University

Satellite altimeter data have been very useful in the study of oceanic eddies. With a growing abundance of satellite data, characterization of the eddy field has greatly expanded. The TOPEX/Poseidon (T/P) altimeter has provided the most accurate sea level variation data to date (*Fu et al.*, 1994). However, the T/P ground track spacing is relatively large (314 km between parallel tracks at the equator) and eddies are only detected while they cross the satellite tracks but are missed when they are between tracks. An example of this problem can be observed in a Gulf of Mexico numerical simulation. In this example, two anticyclonic eddies' cores are between simulated T/P tracks (Fig. 1), so it is not possible to accurately estimate the magnitudes and positions of these eddies applying conventional interpolation methods to the T/P along track sea surface height (SSH) data. In order to identify more features of the eddy field, different processes have been developed to fill the gaps between the tracks (*Hendricks et al.*, 1996; *Jacobs et al.*, 2001).
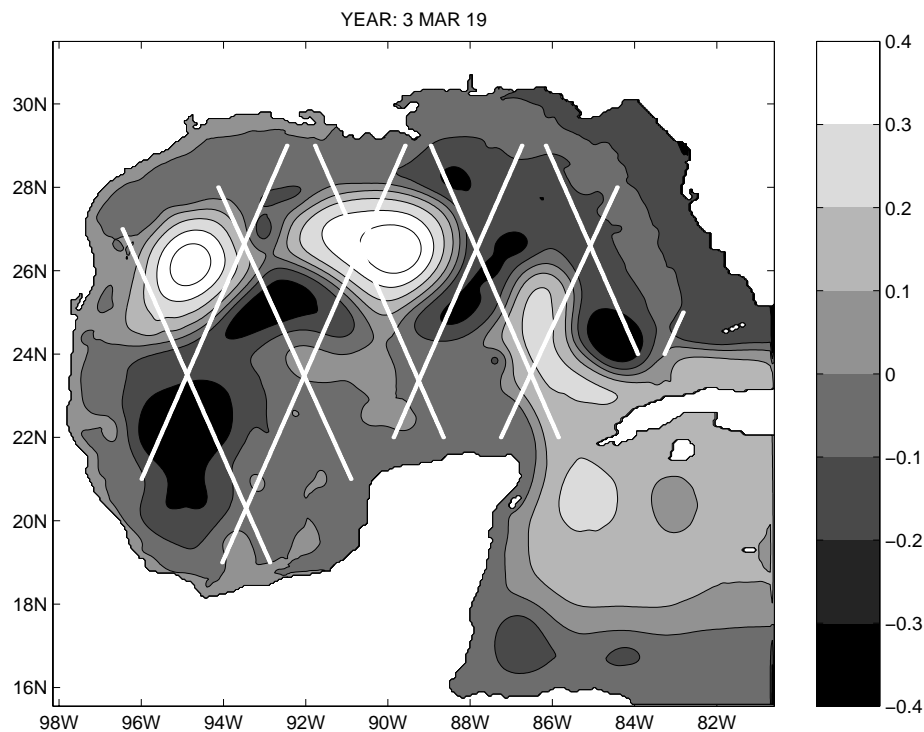

Figure 1. The sea surface height from the COAPS/FSU Gulf of Mexico numerical simulation using the Navy Coastal Ocean Model (NCOM). The white lines are simulated Topex/Poseidon tracks.

Here, a new satellite data processing method that combines propagating empirical orthogonal function (EOF) analysis and an interpolation algorithm based on eigen-modes is tested. The method uses the SSH anomaly data along the tracks, at different times and locations, in order to recognize moving features and recover their position, even at times when they are between tracks. For each EOF mode, space and time information is obtained and interpolated to a high resolution grid. Finally, the field is reconstructed onto the new grid by summing the significant modes.

This technique is applied to two idealized cases: In Experiment One a hypothetical eddy moves eastward. The SSH is sampled periodically along the simulated satellite tracks. Then the technique is applied to interpolate the data in

1 peng@coaps.fsu.edu

space and/or time onto a high resolution grid, recovering the eddy when it is between tracks (Fig. 2). In Experiment Two a synthetic eddy moves in a circle around the center of the domain. The eddy is also well reproduced when it is between tracks (Fig. 2).
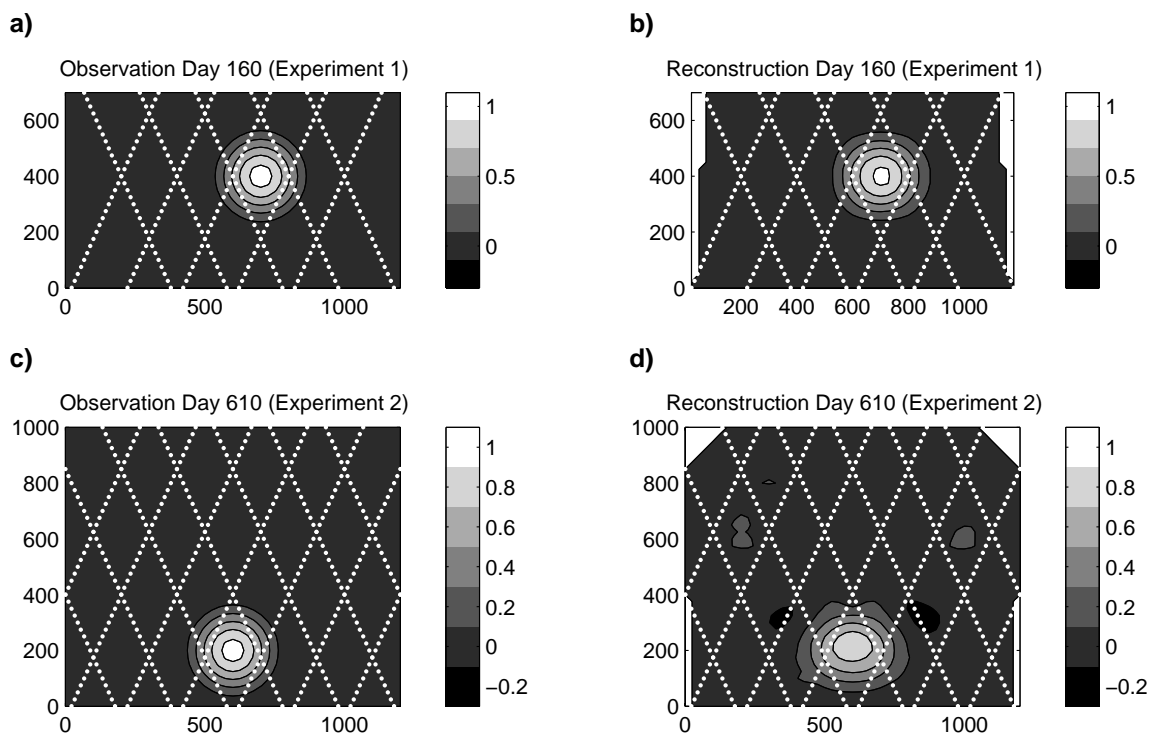
a)

b)

c)

d)

Figure 2. a) The synthetic SSH field for Experiment One with an eddy moving westward; b) The reconstructed field for Experiment One; c) The synthetic SSH field for Experiment Two with an eddy moving anticlockwise around the center of the domain; d) The reconstructed field for Experiment Two. The white dots are simulated satellite tracks.

The real ocean behaves quite differently from these two idealized cases. Usually there is more than one feature within a domain of interest; the data along satellite tracks are not simultaneous, so they have to be synchronized first; data may be missing or erroneous, etc. However, these experiments show that this technique is a promising way to more fully utilize information from the valuable satellite altimeter data. It is also a good candidate for creating SSH fields for numerical model initialization and data assimilation.

Acknowledgements

References

Fu, L. L., E. J. Christensen, C. A. Yamarone, M. Lefebvre, Y. Menard, M. Dorrer, and P. Escudier, TOPEX/Poseidon mission overview, *J. Geophys. Res.*, *99*, 24369–24382, 1994.

Hendricks, J. R., R. R. Leben, G. H. Born, and C. J. Koblinsky, 1996: Empirical orthogonal function analysis of global TOPEX/POSEIDON altimeter data and implications for detection of global sea level rise. *J. Geophys. Res.*, *101*, 14131–14145, 1996.

Jacobs, G. A., C. N. Barron, and R. C. Rhodes, 2001: Mesoscale characteristics. *J. Geophys. Res.*, *106*, 19581–19595, 2001.

Water exchange between the Arctic Ocean and adjacent basins: Essential role of short-term variations

Alexander A. Zelenko and Yurii D. Resnyansky

Hydrometeorological Research Center of the Russian Federation,
Bol. Predtechesky per., 11-13, 123242 Moscow, Russia

E-mail: zelenko@mecom.ru

Mean structure and temporal variability of the water mass exchange between the Arctic Ocean and adjacent basins nave been studied basing on numerical experiments with an ocean general circulation model (*Resnyansky and Zelenko, 1999*). The finite difference scheme of the model source equations was generalized for the computational domain including the near pole neighborhood, which is the singularity point in spherical coordinates.

The numerical experiments have been conducted for the global multiply connected domain (22 internal closed shore contours) including the Arctic Ocean with horizontal grid resolution $\Delta\lambda=\Delta\varphi=1,25°$. The model bathymetry, which also determines the land-sea mask, was constructed on the basis of the WOA-98 electronic atlas. The data from this atlas were also used to specify initial three-dimensional distributions of water temperature and salinity.

The daily atmospheric forcing (wind stress, net heat and fresh water fluxes, i.e. precipitation–evaporation difference) were specified from the meteorological NCEP/NCAR reanalysis data (*Kalnay et al., 1996*) in combination with the relaxation of the computed near-surface water temperature and salinity values to specified distributions from the WOA-98 atlas assuming relaxation coefficient $c_r^{-1} = 30\ d$.

The extent of sea ice was prescribed from daily NCEP data. Dynamic impact of ice on underlying water was allowed for by 20 % reduction of the wind stress vector module exerted on the water surface accompanied by a clockwise rotation of the vector through 20°. Thermodynamic impact was simulated by equating the under ice water temperature to freezing point –1,9°C.

The model has been integrated for several years starting from the state of no motion with climatological temperature and salinity distributions.

The calculations have been reproduced many of the prominent features of large scale water mass exchange of the Arctic Ocean with adjacent basins. Among them, in particular, is such characteristic feature as submerging of West Spitsbergen current under the Arctic surface water as it flows northward (Figure 1). Similar pattern of abrupt submerging is typical of other places of inflow of the Atlantic water under the Arctic surface water.

The pronounced high amplitude short-term variations draw the attention on examination of temporal changes of the net water transport through the straits connecting the Arctic Ocean with adjacent basins. The relationships among different ranges of temporal variability obtained in model simulations (Figure 2) are generally consistent with available direct estimates. In particular, according to evidence of (*Coachman and Aagaard, 1988*), the mean inflow transport through the Bering Strait is about 0.8 *Sv* (1 *Sv* = $10^6\ m^3\ s^{-1}$). This average transport is superimposed by seasonal and interannual variations with amplitude of an order 1 *Sv* and 0.2 *Sv* respectively. But even greater amplitudes are seen for short-term variations. According to (*Coachman, 1993*) they can reach 3.0 *Sv* to the North and 5.0 *Sv* to the South. Similar variability occurs in other passages, through which the Arctic Ocean communicates with neighboring basins, for instance in Fram Strait (Figure 2*b*).

References

Coachman, L.K., 1993: On the flow field in the Chirikov Basin. *Cont. Shelf Res.*, **13**, 481-508.

Coachman, L.K. and K. Aagaard, 1988: Transports through Bering Strait: Annual and inter-annual variability. *J. Geophys. Res.*, **C93**, 15535-15539.

Kalnay, E., M. Kanamitsu, R. Kistler, et al., 1996: The NCEP/NCAR 40-Year Reanalysis Project. *Bulletin of the American Meteorological Society*, **77**, 437-471.

Resnyansky, Yu.D. and A.A. Zelenko, 1999: Effects of synoptic variations of atmospheric forcing in an ocean general circulation model: Direct and indirect manifestations. *Russian Meteorology and Hydrology*, No. 9, 42-50.
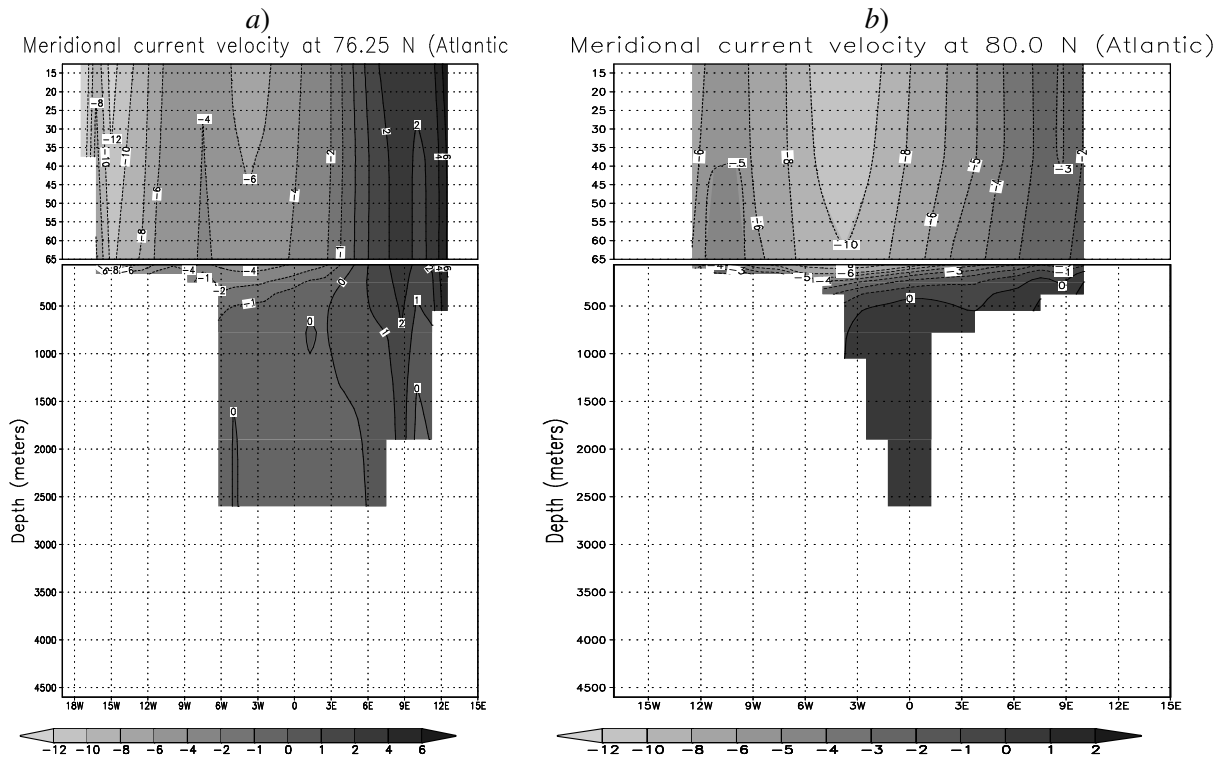
a)
Meridional current velocity at 76.25 N (Atlantic

b)
Meridional current velocity at 80.0 N (Atlantic)

Figure 1. The distribution of the meridional current velocity component ($cm\ s^{-1}$) within two zonal cross-sections through the Fram Strait along latitudes 76.25° N (*a*) and 80° N (*b*).

Note: The velocity is averaged over the last (1997) year of the tree year ocean general circulation model integration on the $1.25° \times 1.25°$ grid within the computation domain involving the North Pole. The northward flow seen at 76.25° N in the surface layers off the western coast of Spitsbergen Island is transformed into the flow submerging within the layer from 500 to 2500 *m* at 80° N.
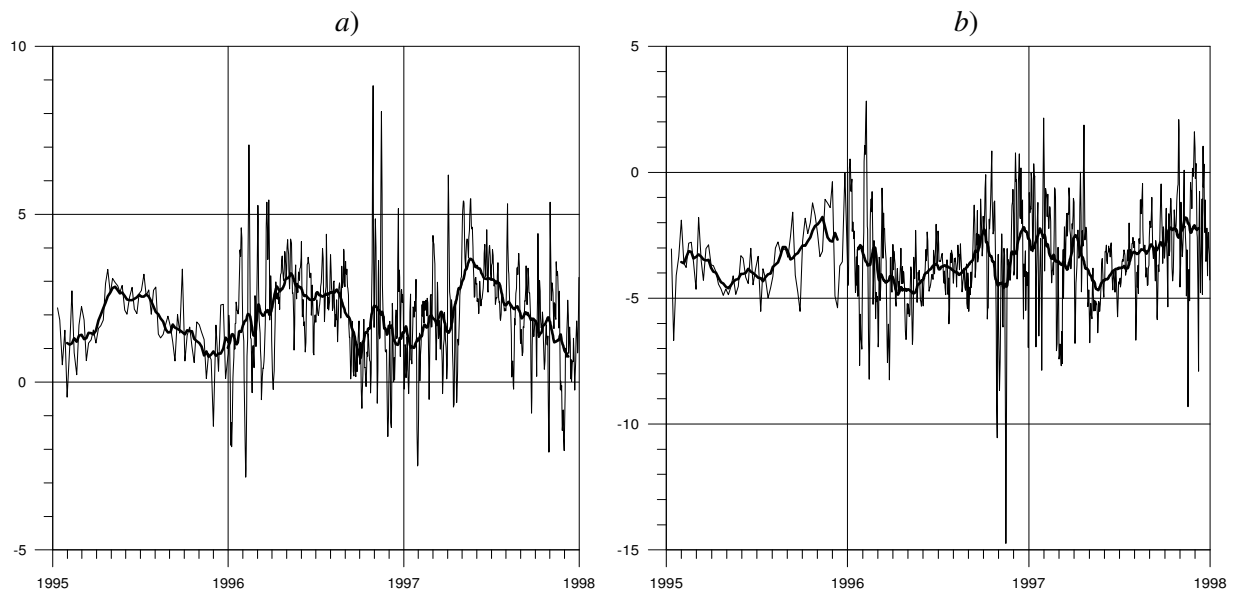

a)

b)

Figure 2. Temporal variations of the overall transports (*Sv*) through Bering Strait (*a*) and Fram Strait (*b*) over three years of model integration with daily atmospheric forcing derived from the NCEP/NCAR reanalysis. Positive values correspond to the northward water transport (from the Pacific to the Arctic Ocean In Bering Strait and from the Atlantic to the Arctic Ocean in Fram Strait). The bold line shows 45 days running mean.